



**WPI**



# Simulation of the Effects of Temperature and Time on the Tempering Behavior of Carburized Steels

A Major Qualifying Project report to be submitted to the faculty of

**WORCESTER POLYTECHNIC INSTITUTE**

in partial fulfillment of the requirements for the Degree of Bachelor of Science

## **Submitted by**

---

Nichole Holman

---

Karen Paklin

---

Shikha Shrestha

## **Submitted on**

May 1, 2014

## **Approved by:**

---

Professor Richard Sisson, Advisor

---

Professor David DiBiasio, Advisor

## Abstract

The heat treating industry needs verified computer simulation tools to predict the carbon concentration profiles and microhardness profiles in carburized steels. Currently tools exist to predict the carbon concentration profiles for many carburization processes including endo-gas and low pressure. The models for the prediction of microhardness profiles as a function of tempering temperatures and times are being developed in this project using experimental results and the Hollomon – Jaffe analysis. The experimental results show that the hardness increases with carbon concentration and decreases with an increase in temperature and time. The results will be used to enhance CarbTool© to predict the microhardness profiles of carburized steel as a function of tempering temperature and time.

## Executive Summary

CarbTool© is a heat treatment simulation program developed by the Center for Heat Treatment Excellence (CHTE). Currently this simulation program predicts the carbon concentration profiles for the carburization process based on the process parameters and physical properties. The objective of this project was to enhance CarbTool© to be able to predict the microhardness profile for the tempering process as a function of time and temperature process parameters. Additionally, Hollomon-Jaffe parameter was utilized to determine the C constant which will be inputted to CarbTool©.

Four steel alloys, AISI 8620, AISI 9310, AISI 1018, and AISI 5120, were chosen for this project because they are widely used in the industry. Initially the alloys were carburized and quenched at Bodycote, after which the carbon concentration data was obtained by Optical Emission Spectroscopy (OES). Then the alloy samples were tempered at five times (1hr, 2hrs, 4hrs, 9hrs and 16hrs) and four temperatures (205°C, 315°C, 425°C, 595°C) in order to replicate tempering conditions in the industry. Following the heat treatment of the alloy samples, they were further prepared for testing by cutting, mounting, grinding, and polishing. The microhardness testing was done using Vickers hardness indentation. Furthermore the samples were etched with 2% nital solution to obtain the photomicrographs using Optical Microscopy.

A number of plots were compiled from the obtained data. Carbon concentration vs. depth was plotted and it was observed that as the depth of the samples increases, the carbon concentration decreases. Next, microhardness vs. depth was plotted which showed that as the depth increases, microhardness decreases. In order to view the trends as time and temperature varied, microhardness vs. depth was plotted for both constant temperature, varying time and constant time, varying temperature. When the time was held constant, the microhardness decreased with increasing temperature and when the temperature was held constant, the microhardness decreased with increasing time. It was observed that the microhardness profile was more affected by varying temperature than varying time. Microhardness was also plotted as a function of the carbon concentration which showed that as the carbon concentration increases, so does the microhardness.

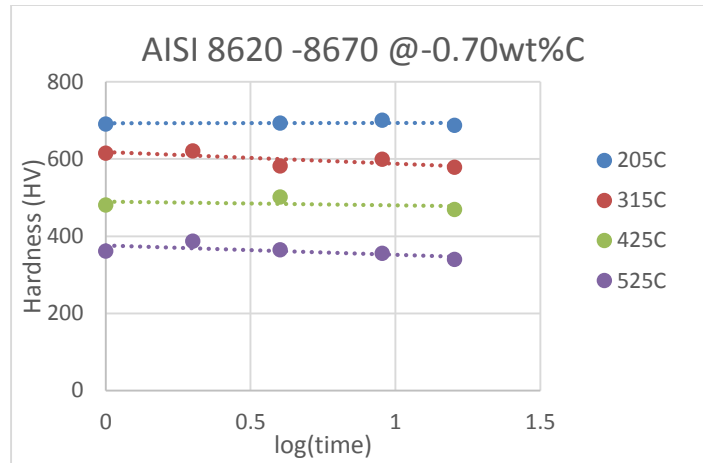


Figure 1: Hardness (HV) vs. log time for AISI 8670.

Using selected carbon concentrations of 0.70, 0.50, and 0.30 wt.%, the Hollomon-Jaffe correlation was used to obtain the linear relations of the hardness for the temperatures shown in Figure 1. Using Mathcad, the team mathematical computed the C constant using the Hollomon-Jaffe parameter shown below for each carbon concentration value.

$$HJP = T[\log(t) + C]$$

These calculated C constants were plotted as a function of the carbon concentration as shown in Figure 2.

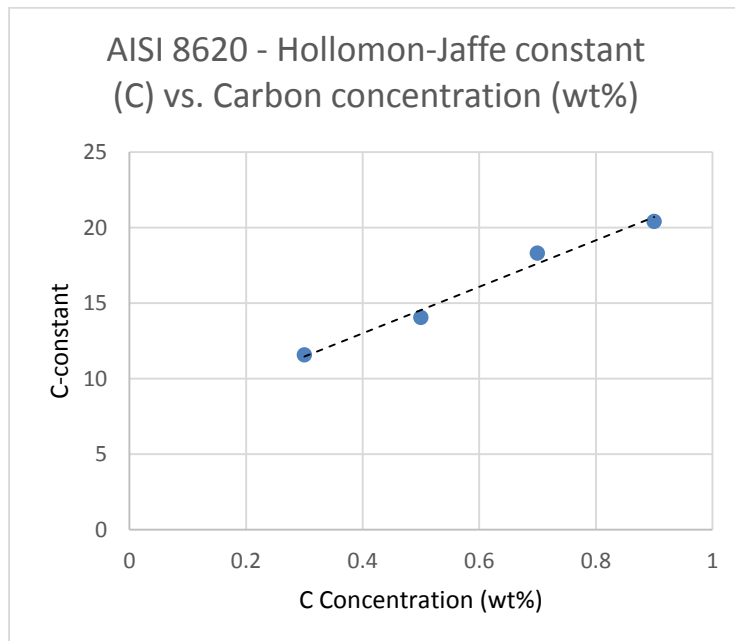


Figure 2: Hollomon-Jaffe constant (C) vs. carbon concentration (wt.%).

After the constant C was determined, this value would be entered into the CarbTool© code along with specific concentration, time and temperature to produce the microhardness profile. Continued work will be done to develop models for the prediction of microhardness profiles as a function of tempering time and temperature. The resulting model from this project can be used for the following:

- Predicting the microhardness profile for tempered steel alloys AISI 1018, AISI 8620, AISI 5120, and AISI 9310.
- Comparison and analysis of the microhardness profile for any time-temperature combination.
- Reduction in the amount of experimental work for industry thus decreasing time to market and cost of any product.
- Overall optimization of the tempering process.

Future work for this project includes further improving CarbTool© to plot the amount of retained austenite as a function of the depth.

## Acknowledgements

We would like to thank a number of people for their support throughout the project. First, we would like to thank our two advisors for their guidance and feedback throughout the project. We extend our thanks to graduate students Lei Zhang and Xiaoqing Cai for training us in using the laboratory equipment and the experimental procedures for tempering, cutting, grinding, polishing, and microhardness testing of the samples in Washburn Laboratories.

Additionally, we would like to thank Professor Boquan Li for his continued assistance in the laboratories while we were performing our experiments and tests. We would like to extend our gratitude to Rita Shilansky, Mechanical Engineering Administrative Assistant for giving us access to the various labs in Washburn and for assisting us with scheduling concerns. Finally, we would like to thank Worcester Polytechnic Institute's Metal Processing Institute (MPI) for allowing us to use the laboratories and Bodycote for carburizing and quenching our samples.

## Table of Contents

Abstract .....	1
Executive Summary .....	2
Acknowledgements .....	5
Table of Contents .....	6
List of Figures .....	9
List of Tables .....	10
Nomenclature .....	11
1.0 Introduction.....	12
2.0 Literature Review.....	13
2.1 CarbTool© .....	13
2.2 Heat Treatment of Steel.....	13
2.2.1 Carburization.....	14
2.2.2 Quenching and Tempering.....	15
2.3 Material Characterization.....	16
2.3.1 Optical Emission Spectroscopy .....	17
2.3.2 X-ray Diffraction for Retained Austenite .....	18
2.3.3 Microstructural Analysis (Optical Microscopy) .....	19
2.4 Microhardness Testing .....	19
2.5 Hollomon-Jaffe Parameter .....	20
3.0 Methodology .....	22
3.1 Carburization and Quenching.....	22
3.2 Tempering .....	22
3.3 X-ray Diffraction for Retained Austenite.....	24
3.4 Preparation of Samples.....	24
3.4.1 Cutting, Mounting, Grinding and Polishing .....	24
3.5 Microhardness Testing .....	26
3.6 Optical Emission Spectroscopy.....	27
3.7 Calculating Hollomon-Jaffe Constant .....	27
3.8 Predicting the CarbTool© Profile .....	27
4.0 Results and Discussion .....	29

4.1	Optical Emission Spectroscopy.....	29
4.2	Tempering Time and Temperature.....	30
4.3	Microhardness Analysis.....	31
4.4	X-ray Diffraction.....	39
4.5	Photomicrograph.....	39
4.6	Hollomon-Jaffe Parameter and Constant C for CarbTool©.....	41
5.0	Conclusion.....	43
6.0	References.....	44
	Appendix.....	47
	Appendix A- Equipment used in Testing and Analysis.....	48
	Appendix A.1: Furnace for Tempering.....	48
	Appendix A.2: Saw used for Cutting.....	48
	Appendix A.3: Sample Mounter.....	48
	Appendix A.4: Grinding and Polishing.....	48
	Appendix A.5: Optical Microscope.....	48
	Appendix A.6: Microhardness Tester.....	49
	Appendix A.7: X-ray Diffraction.....	49
	Appendix B- Experimental Procedures.....	50
	Appendix B.1: Tempering Procedure.....	50
	Appendix B.2: Cutting Procedure.....	51
	Appendix B.3: Sample Preparation Procedure.....	51
	Appendix B.3.1: Mounting.....	51
	Appendix B.3.2: Grinding and Polishing.....	52
	Appendix B.4: Microhardness Analysis Procedure.....	52
	Appendix C- Raw Data.....	53
	Appendix C.1: Carburization Recipe.....	53
	Appendix C.2: Tempering Time-Temperature Data.....	55
	Appendix C.3: Optical Emission Spectroscopy Data.....	64
	OES: AISI 8620.....	64
	OES: AISI 9310.....	65
	OES: AISI 1018.....	66

OES: AISI 5120.....	67
Appendix C.4: Microhardness Data .....	68
Microhardness: AISI 8620.....	68
Microhardness: AISI 9310.....	122
Microhardness: AISI 1018.....	176
Microhardness: AISI 5120.....	185
Appendix C.5: Microhardness Trends .....	194
Microhardness Trends: AISI 8620 .....	194
Microhardness Trends: AISI 9310 .....	242
Appendix C.6: Microhardness and OES vs. Depth Data .....	290
Microhardness and OES vs. Depth: AISI 8620.....	290
Microhardness and OES vs. Depth: AISI 9310.....	299
Microhardness and OES vs. Depth: AISI 1018.....	308
Appendix C.7: Microhardness vs. Carbon Concentration Data .....	310
Microhardness vs. Carbon Concentration: AISI 8620.....	310
Microhardness vs. Carbon Concentration: AISI 9310.....	328
Appendix C.8: Microhardness vs. Carbon Concentration Trends .....	346
Microhardness vs. Carbon Concentration Trends: AISI 8620 .....	346
Microhardness vs. Carbon Concentration Trends: AISI 9310 .....	394
Appendix C.9: Hollomon-Jaffe Data .....	442
Holloman-Jaffe Data: AISI 8620.....	442
Holloman-Jaffe Data: AISI 9310.....	447
Appendix C.10: Mathcad Calculations .....	452
Appendix C.11: C Constants.....	453
Appendix C.12: Photomicrographs .....	456

## List of Figures

Figure 1: Hardness (HV) vs. log time for AISI 8670. ....	3
Figure 2: Hollomon-Jaffe constant (C) vs. carbon concentration (wt.%).....	3
Figure 3: C-Fe phase/ equilibrium diagram for up to 7% carbon (Iron-iron carbide metastable phase diagram, 2013). ....	14
Figure 4: Schematic of optical emission spectrometer (International ASM Handbook Committee, 1986). ....	17
Figure 5: WPI furnace for tempering.....	23
Figure 6: WPI furnace for tempering.....	23
Figure 7: Pace Technologies Nano 2000T Grinder-Polisher in Washburn Laboratories. ....	25
Figure 8: Polisher in Washburn Laboratories. ....	25
Figure 9: Ultrasonic cleaning machine. ....	25
Figure 10: CM-400 AT Micro Indentation Hardness Tester. ....	26
Figure 11: The interface of CarbTool©, gas carburizing process module (Wei et al., 2011). ....	28
Figure 12: Carbon concentration (wt.%) vs. depth (mm) for AISI 8620, experimental and simulation carbon concentration profile. ....	29
Figure 13: Tempering data at a temperature of 205°C for all four samples at different times. ....	31
Figure 14: Microhardness (HV) vs. depth (µm) for sample 8434 – 205°C 1hr.....	32
Figure 15: Microhardness (HV) vs. depth (mm) for AISI 8620, constant time and multiple temperatures.....	33
Figure 16: Microhardness (HV) vs. depth (mm) for AISI 8620, constant temperature and multiple times.....	34
Figure 17: Carbon concentration (wt.%) and microhardness (HV) vs. depth (mm) for samples 8434 – 205°C 1hr. ....	35
Figure 18: Microhardness (HV) vs. carbon concentration (wt.%) for sample 8434 – 205°C 1hr. ....	36
Figure 19: Microhardness (HV) vs. carbon concentration (wt.%) for AISI 8620, constant time and multiple temperatures.....	37
Figure 20: Microhardness (HV) vs. carbon concentration (wt.%) for AISI 8620, constant temperature and multiple times.....	38
Figure 21: X-ray Diffraction for AISI 9310. ....	39
Figure 22: Photomicrograph of AISI 9310 at 5x magnification. ....	40
Figure 23: Photomicrograph of AISI 9310 at 20x magnification. ....	40
Figure 24: Hardness (HV) vs. log time for AISI 8670. ....	41
Figure 25: Hollomon-Jaffe constant (C) vs. carbon concentration (wt.%) for AISI 8620. ....	42

### **List of Tables**

Table 1: Constant value C for varying concentrations of carbon in steel in Hollomon-Jaffe Parameter (Hollomon & Jaffe, 1947).....	20
Table 2: Tempering temperatures and times.....	23
Table 3: Sample alloys for alloy steels tempered at one temperature and different times. ....	30

## Nomenclature

MPI	Metal Processing Institute
CHTE	Center for Heat Treatment Excellence
XRD	X- ray Diffraction
OES	Optical Emission Spectroscopy
RA	Retained Austenite
HJP	Hollomon-Jaffe parameter
WPI	Worcester Polytechnic Institute

## 1.0 Introduction

The Center for Heat Treatment Excellence (CHTE) is an organization that unites industries and universities to research, develop, and improve heat treating processes (Center for Heat Treating Excellence, 2013). CHTE has created a heat treatment simulation program, CarbTool©, to predict the carbon concentration profiles for carburized steels based on the process parameters and physical properties (i.e. carbon diffusivity on a finite of composition, mass transfer coefficients on fluids, density, and phase equilibria). CarbTool© predicts the carbon diffusion at different temperatures to determine the carbon concentration profile of the steel as a function of time (Materials Science & Engineering: Student News – WPI, 2011).

CarbTool© provides alternative methods to alter the amount of carbon in alloyed steel in order to reduce the impurities in those alloyed steels. Currently CarbTool© only predicts the carbon concentration profile for the carburization process and not for the tempering process. The goal is to enhance the capabilities of CarbTool© to also predict the hardness profile (i.e. microhardness vs. distance) as a function of time, temperature, and the constant C from the Hollomon-Jaffe parameter.

Four alloys were selected for testing because they are widely used in the industry to provide a variety of service products ranging from small hand tools, automotive gears, and universal joints to aircraft engine parts, truck transmissions, and large antifriction bearings (Davis, 1996). The alloys were carburized, quenched and tempered to obtain concentration profiles along their core and surface. To obtain the hardness profile, the concentration profiles were utilized and plotted against the case depth. These parameters were inputted in CarbTool© to provide a means of obtaining harder steels, each result dependent on the alloy. This application would allow for more flexibility in applying different heat treatments and visualizing the effect of the hardness of the carbon which would greatly benefit the heat treatment industry.

## 2.0 Literature Review

In this section, we have provided a brief introduction of CarbTool© and its working principle to support our project. Also, the background for methods of the heat treatment of steels implemented for our experiment has been described. Furthermore, we have provided the review on developing the correlation between hardness and carbon concentration as a function of tempering process parameters using the Hollomon-Jaffe equation.

### 2.1 CarbTool©

CarbTool© is an effective software tool for heat treatment developed and verified at CHTE. This software predicts the effect of carburization at different temperatures to determine the carbon concentration profile in the surface and core of the steel as a function of time. Moreover, it is also able to display the optimized cycle time and cost for these steels. The capability of this software is to predict and enhance hardness profile and case microstructure prediction as well as carbon saturation and carbide precipitation simulations. The experimental verification of this carbon profile will be done in the future (Home – Bodycote, 2013).

### 2.2 Heat Treatment of Steel

Steel is an alloy of iron and carbon with the carbon content between a few hundredths of a percent up to about 2 wt.% (Heat Treating, 1991). Using heat treatment processes, the elements in the steel alloy can be manipulated in order to alter the microstructure, and hence their properties. For example, assuming that steels have similar microstructure, as the carbon content in samples of steel are high, then their strength and hardness would increase, however their toughness and ductility would decrease (Hosford, 2005). The heated steel reaches the temperature at which the phase turns to that of austenite. The austenite is then quenched to a low temperature to form a harder form of steel, called martensite, as shown in the Figure 3 phase diagram for up to 7% carbon in steel (Krauss, 2005).

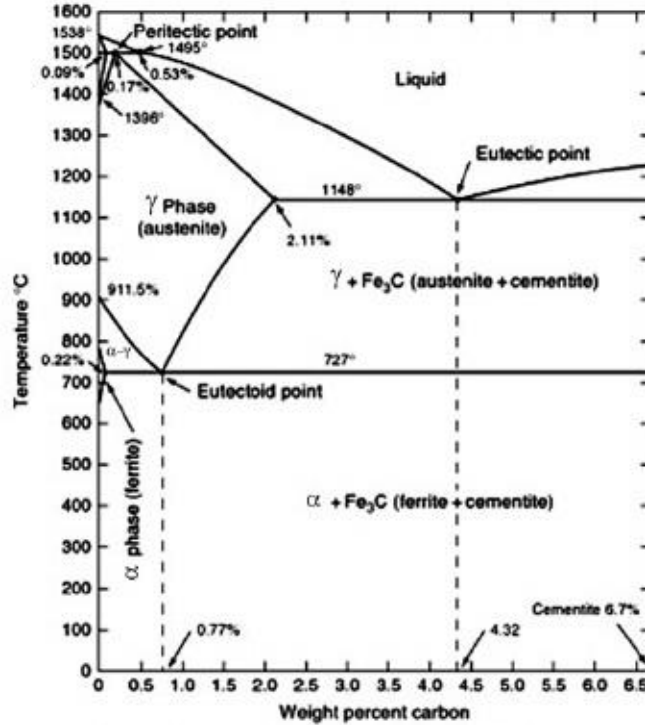


Figure 3: C-Fe phase/ equilibrium diagram for up to 7% carbon (Iron-iron carbide metastable phase diagram, 2013).

However, there might have been some austenite retained in the sample, and the martensite would be tempered in order to get rid of any contributing factors to fatigue, such as austenite, although the austenite may not be completely removed (Krauss, 2005). The methods used for the heat treatment of steel for this experiment are carburization, quenching, and tempering, which are explained in the following sections.

### 2.2.1 Carburization

Carburization is a surface hardening technique for carbon alloys using a thermochemical diffusion process. This method modifies the chemical composition of the desired sample by having a carbon rich atmosphere in a furnace at a temperature high enough to change the phase of the alloy to austenite (Davis, 2002). The difference of the carbon potentials between the atmosphere and that of the desired material provides the driving force to increase the amount of carbon and harden the surface of the steel. The carburization process also provides the benefit of removing and preventing oxidation.

In gas carburization, the furnace atmosphere consists of two gases, where one gas is a carrier, and the other gas is enriched by the carbon. The purpose of the carrier gas is to provide enough positive pressure into the atmosphere in order to minimize the amount of air that enters the furnace. The enriching gas is the gas that provides the rich carbon atmosphere to bring up the amount of carbon on the surface and in the core of the desired steel product (Krauss, 2005). In the case of our experiment, the atmosphere is an endothermic carrier gas, which is produced from methane. The simultaneous reactions occurring due to the endothermic carrier gas would push the carbon to diffuse across the surface of the steel and transform the phase of the desired material to martensite. However, if there is not a sufficient amount of carbon in the atmosphere of the furnace, then there will be no driving force for the carbon to transfer from the endo-gas to the desired material. Additionally, if there is too much carbon in the atmosphere of the furnace, then several complications may occur, such as an overabundance of retained austenite, leaving the martensite brittle (Krauss, 2005). In order to prevent this from occurring, the carbon content of the carburized steel is limited to about 0.8 to 1% and the temperature during the carburization process is between 850°C to 950°C (Davis, 2002).

After the carburization process, the austenite would be quenched in an oil bath in order to form martensite (Krauss, 2005). After quenching, the steel is tempered to improve the ductility and toughness (Davis, 2002).

### **2.2.2 Quenching and Tempering**

Typically for steels, the as-quenched form is not used because it is fully hardened and therefore is extremely brittle and has a low toughness. Instead, in order to make tough parts, the combination of the quenching process and the tempering process is used to create tough, usable parts where tempering is used to relieve the stress that results from the quenching process (Metal Hardening / Metal Quenching / Metal Tempering, 2012). In general, the heat treating process involves both quenching, to fully harden the part, and tempering, to achieve the desired final hardness and toughness.

Quenching is a process that “provides a mean to control mechanical properties of steels as tensile strength, toughness and hardness” (Oliveira, Savi, & Pacheco, 2013). This process involves heating the material to a pre-determined temperature, then immersion in a quenchant in

order to quickly cool the part to a fully hardened state (Metal Hardening / Metal Quenching / Metal Tempering, 2012). In this project, the quenchant used was oil. High residual stress from quenching can result in a “combination of phase transformations, large temperature gradients and non-uniform cooling” (Oliveira et. al., 2013). Tempering is performed to remove the residual stresses.

Tempering is a process that follows quenching in order to obtain a desired “hardness/toughness ratio” (Tempering, 2013). It can lower the hardness of the material to within a desired range or can allow the material to meet “certain mechanical property requirements” (Metal Hardening / Metal Quenching / Metal Tempering, 2012). There are many ways to temper a material including molten metal baths, oil baths, salt baths, and flame or induction heating units. The most common method of tempering, and the method that we are using is in a convection air furnace. Tempering times and temperatures are chosen in order to end up with the desired properties in the steel; these times and temperatures should be chosen carefully based on the required properties. If the tempering times and temperatures are chosen correctly, the resulting part has the “appropriate combination of hardness, strength and toughness for the intended application” (Metal Hardening / Metal Quenching / Metal Tempering, 2012). Based on the material specifications, the tempering temperature can range from 160°C to 500°C or higher. In conclusion, the benefit of tempering is to fine-tune the steel properties such as hardness and toughness to fit application requirements or desires (Tempering, 2013).

## **2.3 Material Characterization**

Material Characterization refers to the use of techniques to probe into the internal structure and properties of a material. This takes place in actual materials testing or analysis form. These techniques help us know more about the behavior of the specimen and its internal structure. The analysis can be done using different types of microscopes such as optical microscopes, scanning electron microscopes, transmission electron microscopes or the elemental analysis of the specimen can be done using X-ray Diffraction (XRD). In the next sections, the methods used for material characterization for this project are explained in detail.

### 2.3.1 Optical Emission Spectroscopy

Optical Emission Spectroscopy (OES) is a method used for qualitative and quantitative elemental analyses of elements in metals and alloys. In this method, the energy is provided by striking an electrical arc to the surface of the sample where a small portion of the sample is vaporized. This ionizes and excites the atoms, creating an emission spectrum specific to each element. The light emitted is analyzed by diffraction grating to separate it into its various component wavelengths. The resulting spectrum is recorded and compared to the spectra of known elements to determine the elements present. Quantitative determination of the concentration of each element is done by comparing the intensities from the unknown sample with their counterparts from a series of standards of known concentration. The limitations for OES are that it cannot analyze elements such as hydrogen, oxygen, nitrogen, halogens and noble gases quantitatively. Carbon and sulfur can only be measured in instruments equipped with vacuum chambers and in cases where the sample has not been powdered and mixed with these elements. For our experiment, we used OES in order to determine the carbon concentration in our alloys in the presence of Argon gas (International ASM Handbook Committee, 1986). The schematic for the OES can be seen in Figure 4.

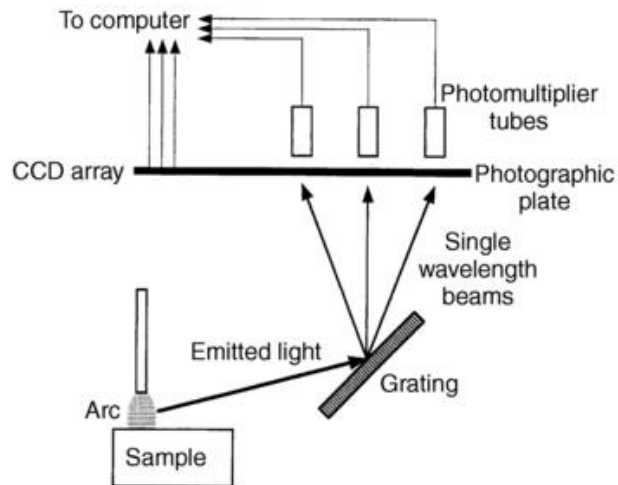


Figure 4: Schematic of optical emission spectrometer (International ASM Handbook Committee, 1986).

### 2.3.2 X-ray Diffraction for Retained Austenite

X-ray Diffraction (XRD) is a characterization method for crystalline materials such as steel. When an X-ray beam is directed at the sample, a number of beams emerge at certain angles providing the information about the geometry, orientations, and arrangements of atoms in the crystal that make up the sample. This incident X-ray consists of electromagnetic radiation and its interaction with the sample produces constructive interference and a peak in intensity occurs. However, this happens only if Bragg's law is satisfied which is given by equation 1:

$$n\lambda = 2d\sin\theta \quad (1)$$

Where  $n$  is any integer,  $\lambda$  is the wavelength of incident and diffracted beams,  $d$  is the spacing of adjacent diffracting planes in the crystalline sample, and  $\theta$  is the angle between the diffracting plane and the incident beam. The diffracted X-rays are then detected and recorded. The conversion of the diffraction peaks to d-spacing allows identification of the sample, as all the samples have a set of unique d-spacing. This is achieved by comparison of d-spacing with standard reference patterns. XRD is typically used for identification of phases or compounds present in metals, ceramics etcetera, or quantitative determination of fractions of each phase in multi-phase mixtures, such as retained austenite in steel (American Society for Testing and Materials International, 2014).

In our experiment we used X-ray Diffraction for retained austenite. The retained austenite (RA) is the austenite that does not transform to martensite upon quenching; retained austenite occurs when steel is not quenched to the martensite finish ( $M_f$ ) temperature i.e. low enough to form 100% martensite (Herring, 2005). The amount of retained austenite is a function of the carbon content, alloy content, quenchant temperature, and subsequent thermal and/or mechanical treatments (Pappas, 2006). Depending on the steel chemistry and specific heat treatment, the retained austenite level in the case can vary from over 50% of the structure to nearly 0%. While large amounts of retained austenite can be detected and estimated by optical microscopy, specialized equipment and techniques, such as X-ray Diffraction methods, are required to accurately measure the amount of retained austenite to as low as 0.5%. XRD determines the retained austenite phase in steel using integrated intensities (area under peak above background) of X-ray Diffraction peaks using chromium  $K_\alpha$  X-radiation (Magner et al., 2002).

### 2.3.3 Microstructural Analysis (Optical Microscopy)

Optical Microscopy is the process of determining the characteristics of the material by using an optical microscope, which is made up of lenses that magnify and focus light. The light may be transmitted through the material or reflected from a material's surface. Optical microscopy can be used to evaluate the material's compositions, either single or multiple phases, and structure using the photomicrograph that it produces. In this project, optical microscopy was performed on the alloys to study their various regions of microstructure.

### 2.4 Microhardness Testing

Microhardness refers to the indentation hardness tests made with loads not exceeding 1kg. In general, the term is related to the size of the indentation rather than the load applied. Microhardness testing is performed with either the Knoop or the Vickers indenter. In our experiment, we used Vickers indenter to test the microhardness of the alloy samples. The procedure for testing is very similar to that of the standard Vickers hardness test, except that it is done on a microscopic scale with higher precision instruments. The surface being tested generally requires a metallographic finish; the smaller the load used, the higher the surface finish required. In this test, the indenter is a square-based diamond pyramid that allows evaluation of the material and has the very important advantage of placing the hardness of materials on one continuous scale. The load is applied smoothly, without impact, and held in place for 10 or 15 seconds. After the load is removed, the two impression diagonals are measured, usually with a filar micrometer, to the nearest 0.1  $\mu\text{m}$  and then averaged. The Vickers hardness (HV) is calculated by equation 2 where the load  $L$  is in grams-force, and the average diagonal  $d$  is in  $\mu\text{m}$ .

$$HV = \frac{1854.4L}{d^2} \quad (2)$$

Microhardness testing is the best method in present use for accurately determining case depth and certain case conditions of carburized or nitrided work pieces. In most instances this is accomplished by use of test coupons that have accompanied the actual work piece through the heat treating operation. The coupons are then sectioned and usually mounted for testing.

## 2.5 Hollomon-Jaffe Parameter

The Hollomon-Jaffe parameter, also known as the tempering parameter, similar to the Larson-Miller parameter, is used during tempering to “define time-temperature equivalences” (Virtanen et al., 2013; Metallurgy; Findings from C. Gomes and Co-Researchers Advance Knowledge in Metallurgy, 2011). It gives the time-temperature correlation between low temperature, long tempering time, and high temperature, short tempering time (Black, Cook, Loveless, Rudnev, & Weiss, 1999). Low temperature, and a long tempering time achieves the same effect as high temperature and a short tempering time. During steel tempering, the Hollomon-Jaffe parameter also describes the change in the hardness of the material (Virtanen et al., 2013). The Hollomon-Jaffe equation is given in equation 3.

$$HJP = T[\log(t) + C] \quad (3)$$

In the Hollomon-Jaffe equation,  $HJP$  is the Hollomon-Jaffe parameter,  $T$  is the tempering temperature in Kelvin,  $t$  is time in hours, and  $C$  is a unitless constant that is dependent on the material being tempered (Kamp, Celotto, & Hanlon, 2012).

There is another variation to the Hollomon-Jaffe parameter which can be used to compare how a sample of steel responds to the process of tempering using time and temperature, as shown in equation 4.

$$HJP = \frac{T[\log(t)+C]}{1000} \quad (4)$$

The constant  $C$ , as determined by Hollomon and Jaffe, varies linearly for carbon concentrations between 0.3 and 1.10%. This constant is equivalent to different values as summarized in Table 1.

Table 1: Constant value  $C$  for varying concentrations of carbon in steel in Hollomon-Jaffe Parameter (Hollomon & Jaffe, 1947).

<b>Constant Value, C</b>	15	19.5	20	30
<b>Carbon Content in Steels (%)</b>	0.90-1.20	0.15-0.45	C-Mn and low alloy steels	High alloy steels

If the heating and cooling cycles were to be included in the Hollomon-Jaffe parameter, then the formula would be rearranged in a manner as shown in equation 5.

$$HJP = \frac{T[\log(\tau)+20]}{1000} \quad (5)$$

In the equation,  $\tau$  is the residence time within the tempering process. This can then be manipulated to determine if there is an alternative temperature that may be used to achieve similar results.

$$\tau = t + \frac{T}{(2.3*K_1(20-\log(K_1)))} + \frac{T}{(2.3*K_2(20-\log(K_2)))} \quad (6)$$

In equation 6,  $K_1$  and  $K_2$  are the heating rate and cooling rate respectively in Kelvin/hour (Hollomon & Jaffe, 1947).

### **3.0 Methodology**

The goal of this project was to improve the software CarbTool© with the addition of tempering parameters. There were various stages that the samples needed to go through in order to accomplish our ultimate project objective. These tasks included:

- 1) Carburization and Quenching
- 2) Tempering
- 3) X-ray Diffraction
- 4) Optical Emission Spectroscopy
- 5) Entering the data into CarbTool©

#### **3.1 Carburization and Quenching**

Alloy samples of AISI 8620, AISI 9310, AISI 1018, and AISI 5120 were carburized at Bodycote and the resulting correlations will be entered as code into the developing computer software that was developed by hard working students of Worcester Polytechnic Institute (WPI), who are recognized in the acknowledgement section of this report. The carburization recipe can be found in Appendix C.1: Carburization Recipe. After the carburization process, the samples were quenched in oil at Bodycote.

#### **3.2 Tempering**

According to literature values, the hardness is more affected by temperature than by time, thus from a range of temperatures most often tempered 160°C to 500°C, or higher, intervals were selected for which to conduct the microhardness analysis (Tempering, 2013). Based on the literature review, we chose a range for the optimal values and selected intervals as shown in Table 2.

Table 2: Tempering temperatures and times.

Temperature (°C)	Time (Hours)				
	1	2	4	9	16
205	X <sub>11</sub>	X <sub>12</sub>	X <sub>13</sub>	X <sub>14</sub>	X <sub>15</sub>
315	X <sub>21</sub>	X <sub>22</sub>	X <sub>23</sub>	X <sub>24</sub>	X <sub>25</sub>
425	X <sub>31</sub>	X <sub>32</sub>	X <sub>33</sub>	X <sub>34</sub>	X <sub>35</sub>
595	X <sub>41</sub>	X <sub>42</sub>	X <sub>43</sub>	X <sub>44</sub>	X <sub>45</sub>

Table 2 shows the different temperatures of the furnace and the different times of the tempering process for our experiments. For tempering, the temperatures measured from the furnace may be different depending on whether the heating is equally distributed. Thus, a thermocouple was used to calibrate the furnace and if there were discrepancies between the temperature in the furnace and the readings of the thermocouple, the temperature of the furnace was adjusted accordingly. To reduce any inaccuracies, a small hole was drilled into an extra sample to allow the thermocouple to accurately read the temperature of the samples. The furnace used for this process is shown in Figure 5 and in Figure 6.



Figure 5: WPI furnace for tempering.



Figure 6: WPI furnace for tempering.

The three stages of tempering are the heating, the holding, and the cooling of the sample. For each temperature and time, the furnace was set to the desired temperature. During heating, when the furnace temperature indicator showed twenty degrees lower than the desired temperature, the samples were placed in the furnace. This was the heating stage. The holding stage began as soon as the samples are placed in the furnace and ran for the duration of the desired time. After the holding stage, the samples were taken out of the furnace and left in ambient temperature for the cooling stage.

### **3.3 X-ray Diffraction for Retained Austenite**

X-ray Diffraction was done using an Empyrean Multi-Purpose Research X-ray Diffractometer XRD by PANalytical in Washburn Laboratories at WPI.

### **3.4 Preparation of Samples**

In the following section the procedural steps for preparing the samples before implementing microhardness testing, such as cutting, mounting, grinding and polishing have been provided.

#### **3.4.1 Cutting, Mounting, Grinding and Polishing**

After tempering the samples for four different times and five different temperatures, each sample was cut in order to expose a cross section on which microhardness testing could be done. For this, a red alumina saw was used to cut all the alloys.

After the samples were cut, they were mounted to be able to perform microhardness testing on them. For this, the samples were placed in a Buehler SimpliMet 3000 automatic mounting press, then the thermoplastic resin (phenolic powder) was added and the samples were processed under heat and high pressure. Due to heat and pressure, the powder melted and formed a plastic case without affecting the sample (Buehler, 2007).

The next step was grinding and polishing the mounted samples in order to get accurate data for microhardness testing. The objective was to produce a sample that is “scratch free and mirror-like in appearance” (Buehler, 2007). The samples were initially grinded using a manual

technique on a Pace Technologies Nano 2000T Grinder-Polisher seen in Figure 7. The initial grinding was done by using the Silicon Carbide (SiC) abrasive grit 180, followed by 400, 600 and 1200. This sequence was in terms of decreasing the abrasive grit particle size to obtain surface finishes that were ready for polishing. The samples were grinded against the sandpaper. After grinding, polishing was done by using an aqueous alumina solution of 1.0 micron to ensure a smoother surface finish on the sample. The polishing machine that was used can be seen in Figure 8 (NANO 2000 Polisher, 2011).



Figure 7: Pace Technologies Nano 2000T Grinder-Polisher in Washburn Laboratories.

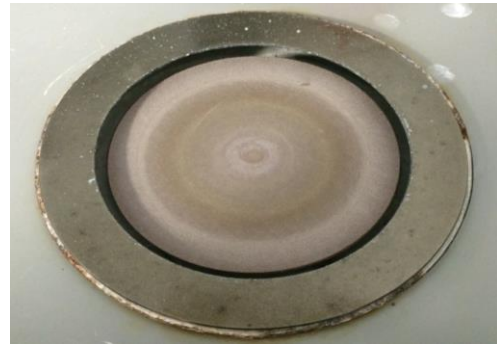


Figure 8: Polisher in Washburn Laboratories.

The final step was ultrasonic cleaning, seen in Figure 9, which removed the unwanted debris and bubbles caused by drying of the acetone that was used to clean the samples.



Figure 9: Ultrasonic cleaning machine.

### 3.5 Microhardness Testing

The microhardness measurement of the polished alloy samples was done using a Vickers microhardness tester on a Clark, CM-400 AT using a 200 gm load for a dwell time of 10 seconds. Figure 10 shows the microhardness machine used during this project.



Figure 10: CM-400 AT Micro Indentation Hardness Tester.

The samples were placed in the microscope and the microhardness measurements were made using a Vickers indenter. In order to determine which edge of the sample to measure the hardness at, indentations were made on adjacent edges of the sample and the reading for hardness was taken. The opposite side of the edges had approximately the same hardness, hence the adjacent edges were read. The edge having the highest hardness reading was chosen for making indentation lines and for measuring the microhardness of the sample. The first indentation was made on the edge of the sample and subsequent indentations were made at a distance of approximately 104  $\mu\text{m}$  from the previous diamond indentation. Two lines of indentations were made on each sample in which twenty five indentations were made for each line. The microhardness of all indentations was measured by all three teammates in order to obtain accurate data. The final hardness for each indentation for each sample was determined by averaging the data read by all three members of the team.

### 3.6 Optical Emission Spectroscopy

Optical Emission Spectroscopy was done on the as-quenched, AISI 8620, AISI 9310, AISI 1018, and AISI 5120 samples to measure the carbon concentration. The measurements were done to obtain the carbon concentration profile (carbon concentration vs. depth) on the surface of the sample. After each measurement, the samples were grinded to decrease the depth and then carbon concentration was measured again on the surface. Carbon concentration measurements were taken at four different locations on the surface of each layer.

### 3.7 Calculating Hollomon-Jaffe Constant

The Hollomon-Jaffe parameter is given by equation 7.

$$HJP = T[\log(t) + C] \quad (7)$$

It is the function of time, temperature, and Hollomon-Jaffe constant C. Hardness is also the function of time and temperature, which is given by equation 8:

$$Hardness = f(T[\log(t) + C]) \quad (8)$$

Hence, there exists the functional relationship between hardness and the Hollomon-Jaffe parameter. Therefore, to calculate the Hollomon-Jaffe constant C at different concentrations for steel, different combinations of time and temperatures are determined that produced the same hardness. Then the time and temperatures are plugged into equation 9 below (Hollomon & Jaffe, 1945).

$$C = - \left[ \frac{T_1 \log t_1 - T_2 \log t_2}{T_1 - T_2} \right] \quad (9)$$

After we get the value of constant C, we enter this value in the CarbTool© code, with specific concentration, time, and temperature to produce the microhardness profile.

### 3.8 Predicting the CarbTool© Profile

In this project, the simulation tool CarbTool©, has been used for the calculation of carbon concentration profile during carburizing process where the user input parameters are carburization temperature, carburizing time, and carbon potential or flux. After a quick

simulation, the carbon profile along the distance below the surface can be plotted with the case depth. In this section we have presented the outputs of CarbTool©, which are the carbon concentration distribution profile inside the steel part and the surface which was done by WPI students in previous years. The interface for the carburizing process that was created by the previous students using CarbTool© is shown in Figure 11. We used the profile as a reference to predict our data points and plots.

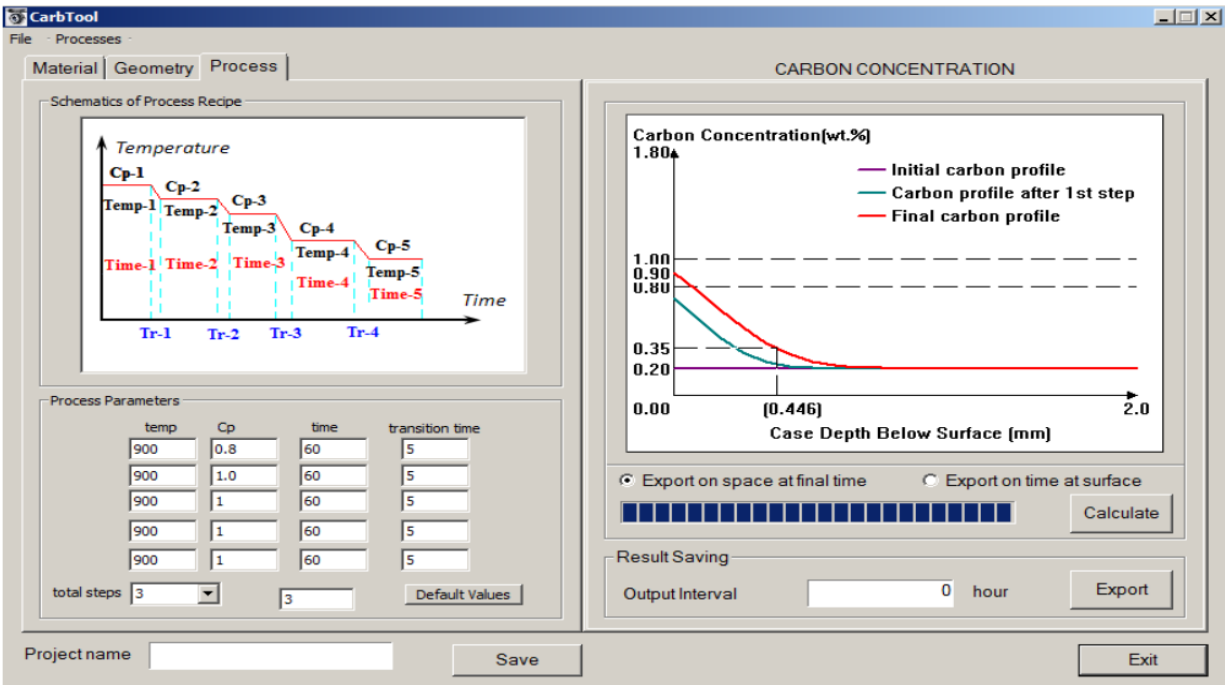


Figure 11: The interface of CarbTool©, gas carburizing process module (Wei et al., 2011).

## 4.0 Results and Discussion

The elemental concentrations were determined using optical emission spectroscopy to obtain the carbon concentration profiles. CarbTool© was then used to predict that carbon concentration profile alongside the experimental analysis. The samples were then prepared by cutting, mounting, grinding, and polishing to obtain the microhardness. Mathematical analysis permitted the use of the Hollomon-Jaffe parameter to obtain the C constants for alloys AISI 8620 and AISI 9310.

### 4.1 Optical Emission Spectroscopy

The alloys analyzed were carburized at Bodycote, the recipe of which can be seen in Appendix C.1: Carburization Recipe. After the as-carburized and as-quenched alloys were received from Bodycote, one sample of each carburized alloy was analyzed to obtain the respective carbon concentration profile. The carbon-depth profile measurements were performed using the Optical Emission Spectroscopy (OES) and the graph was plotted. Then the results were compared with the prediction of CarbTool©, which is shown below in Figure 12.

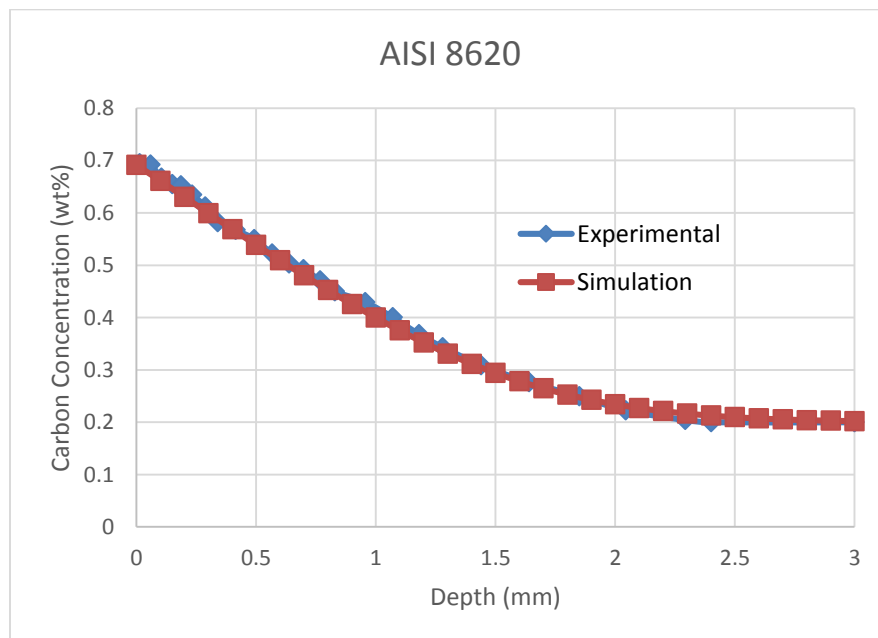


Figure 12: Carbon concentration (wt.%) vs. depth (mm) for AISI 8620, experimental and simulation carbon concentration profile.

To view the other OES graphs for AISI 9310, AISI 1018, and AISI 5120, please refer to Appendix C.3: Optical Emission Spectroscopy Data.

## 4.2 Tempering Time and Temperature

All the alloy samples of AISI 8620, AISI 9310, AISI 1018, and AISI 5120 were tempered at five times (1hr, 2hrs, 4hrs, 9hrs and 16hrs) and four temperatures (205°C, 315°C, 425°C, 595°C) as shown in Appendix C.2: Tempering Time-Temperature Data. Table 3 shows an example of the sample numbers respective to each alloy tempered at one temperature and different times. A full list of the samples tempered can be found in Appendix C.2: Tempering Time-Temperature Data.

Table 3: Sample alloys for alloy steels tempered at one temperature and different times.

Temperature (°C)	Time (Hr)	AISI 1018	AISI 8620	AISI 5120	AISI 9310
<b>205</b>	<b>1</b>	1427	8434	5421	9048
	<b>2</b>	-	-	-	-
	<b>4</b>	1436	8428	5424	9052
	<b>9</b>	1433	8446	5435	9043
	<b>16</b>	1444	8440	5429	9007

The tempering for the temperature of 205°C, 2 hours was not completed because there were no more spare samples of AISI 9310 to temper. The alloy AISI 9310 is an expensive alloy and the amount of steel mills available with the product is limited. In the future, perhaps this one tempering time and temperature may be completed.

While tempering, the data for temperature was collected at five minute increments to visualize the change in the temperature until it was constant. Figure 13 shows the tempering data and trend at 205°C for varying times. More tempering data and graphs are enlisted in Appendix C.2: Tempering Time-Temperature Data.

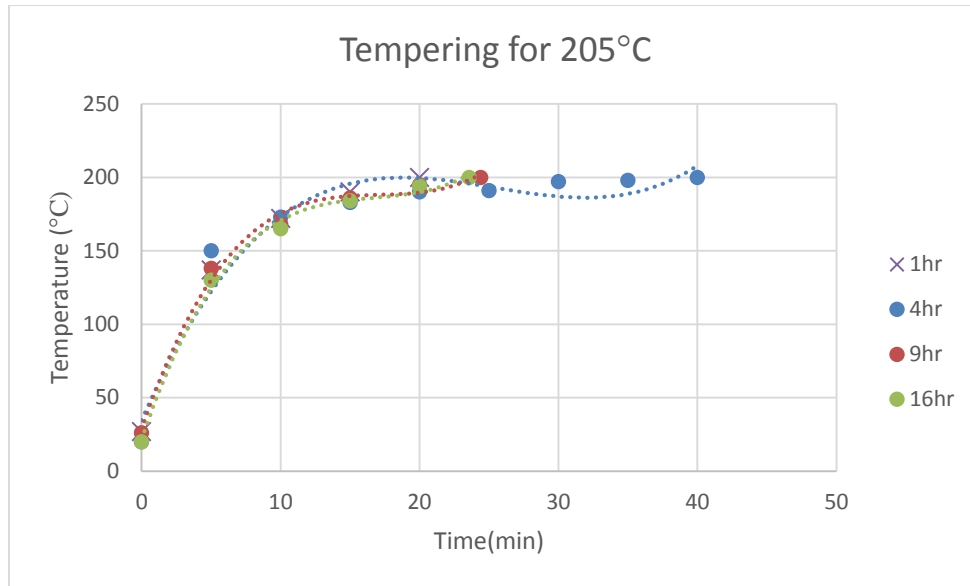


Figure 13: Tempering data at a temperature of 205°C for all four samples at different times.

The trends in the graph above display that as time increases, the temperature also increases greatly within the first twenty minutes before evening out to the temperature that the furnace was set to. Any discrepancy in the data collected for tempering might be due to the furnace having been previously set to a higher temperature and retaining enough heat to reach the set temperature at a quicker rate than if it had not been previously set to a higher temperature. The heating times were determined to be 18 minutes.

### 4.3 Microhardness Analysis

As a reminder, to complete the microhardness analysis, each sample alloy had two lines of indentations, each line with approximately twenty-five points. To ensure correct data, each of the three group members completed their own readings. After all three group members read both indentation lines, the microhardness was plotted against the depth, as shown in Figure 14. A best-fit polynomial trend was then applied where the equation for Run 1 (Line 1) is above and equation for Run 2 (Line 2) is below. The  $R^2$  values signify how close the best-fit line is to the experimental results. The closer the  $R^2$  value is to 1, the more reliable the trend.

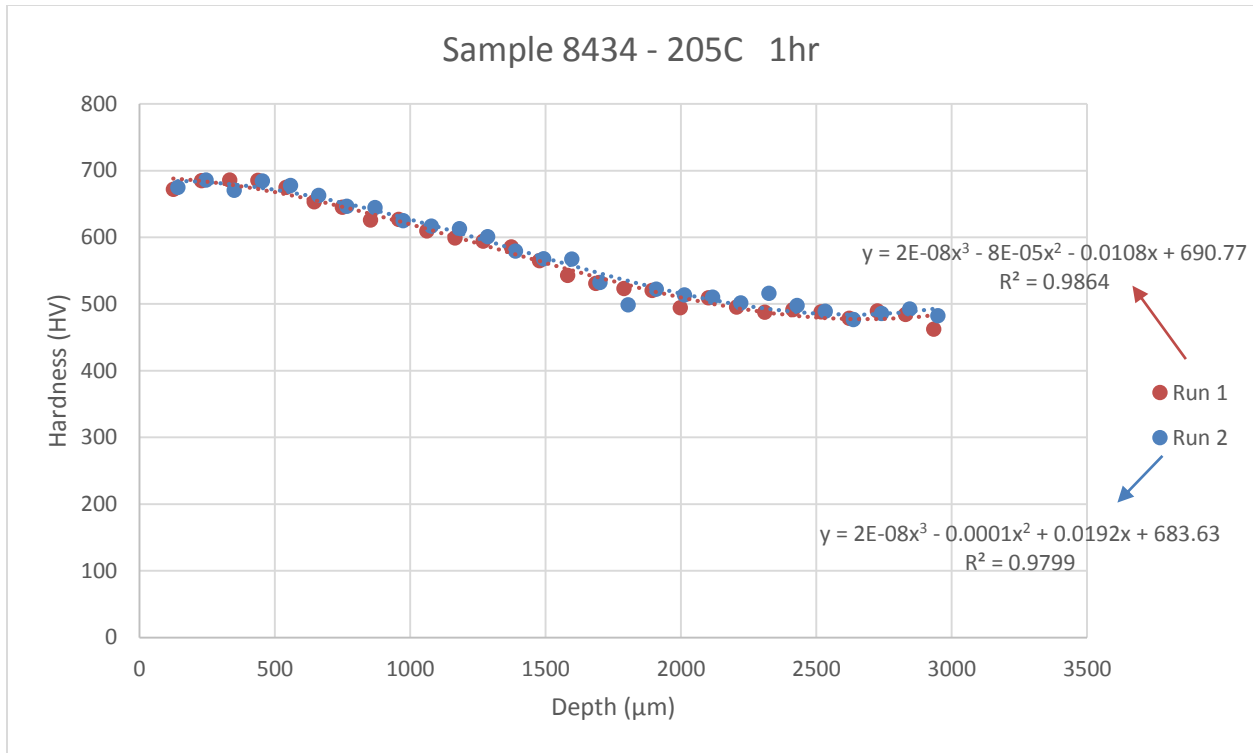


Figure 14: Microhardness (HV) vs. depth ( $\mu\text{m}$ ) for sample 8434 – 205°C 1hr.

The microhardness analysis was conducted mostly for alloys AISI 8620 and AISI 9310. These alloys were prioritized in the completion of the analysis because they are most often used in the industry, ranging from small gears to industrial aircraft parts. For a list of the microhardness analysis for all samples completed, please refer to Appendix C.4: Microhardness Data. In order to obtain a precise line, outlier points were omitted. These outlier points were most likely caused either by the cutting machine or by vibrations while indenting the sample. The cutting machine could have created the arbitrary points if the sample was cut too quickly, it would act to further temper the sample in certain locations. Additionally, there was a concern with the alloy AISI 9310 for retained austenite. If it was displayed that there was a large enough hump close to the edge of the sample, then it would signify the presence of retained austenite.

Other samples that underwent the microhardness analysis were the as-quenched samples for a comparative analysis. Trends were correlated in order to confirm that the experimental results agreed with the literature trends. Two trends that were analyzed were the microhardness obtained for a constant time and multiple temperatures, then again for a constant temperature and

multiple times for alloys AISI 8620 and AISI 9310. These trends can be found in Appendix C.5: Microhardness Trends. Below is an example of the trends for AISI 8620 at a constant time and multiple temperatures in Figure 15 and at a constant temperature and multiple times in Figure 16.

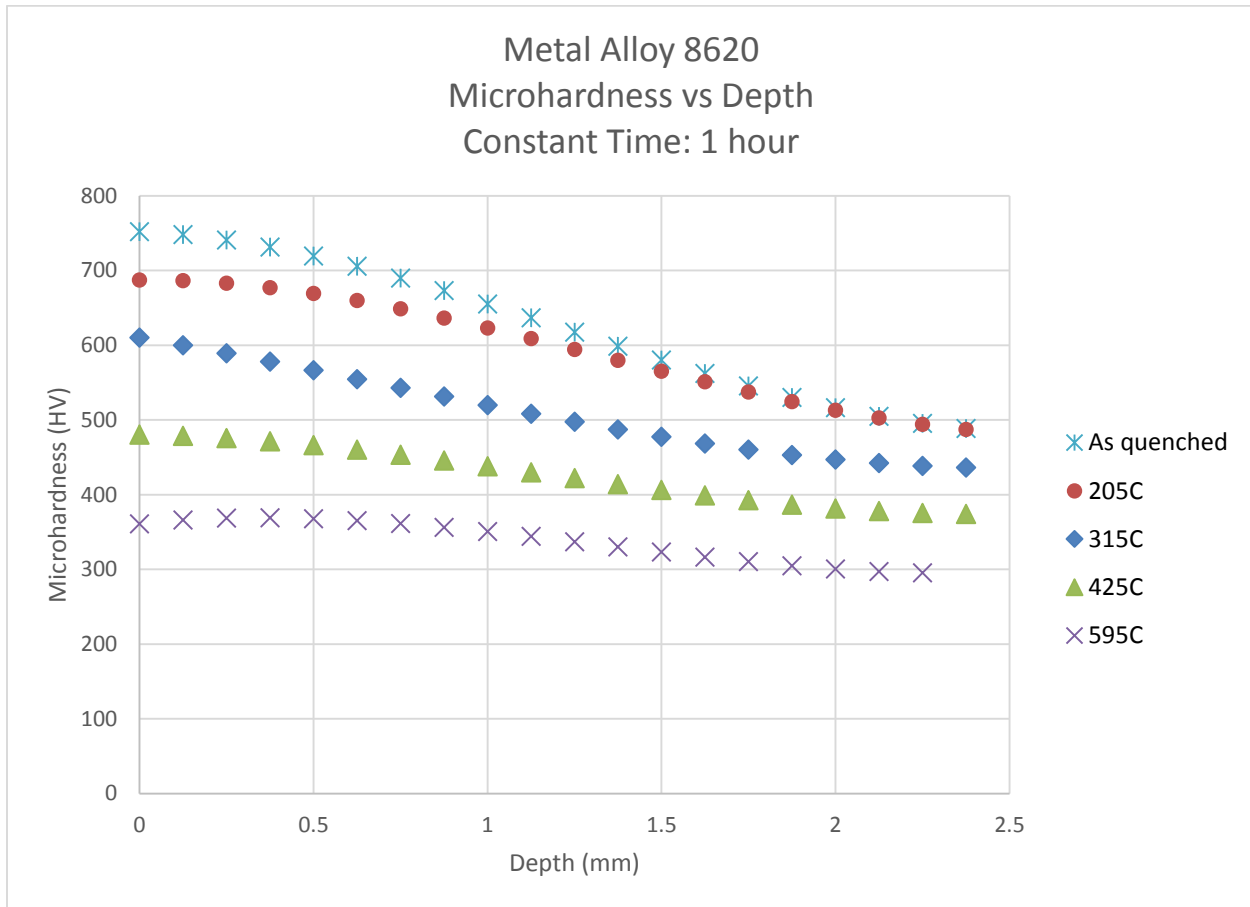


Figure 15: Microhardness (HV) vs. depth (mm) for AISI 8620, constant time and multiple temperatures.

The trends agree with the literature values in which as the depth of the sample increases, the hardness will decrease. However, the microhardness is at its highest for the as-quenched sample alloy and decreases as the temperature of the tempered alloy increases.

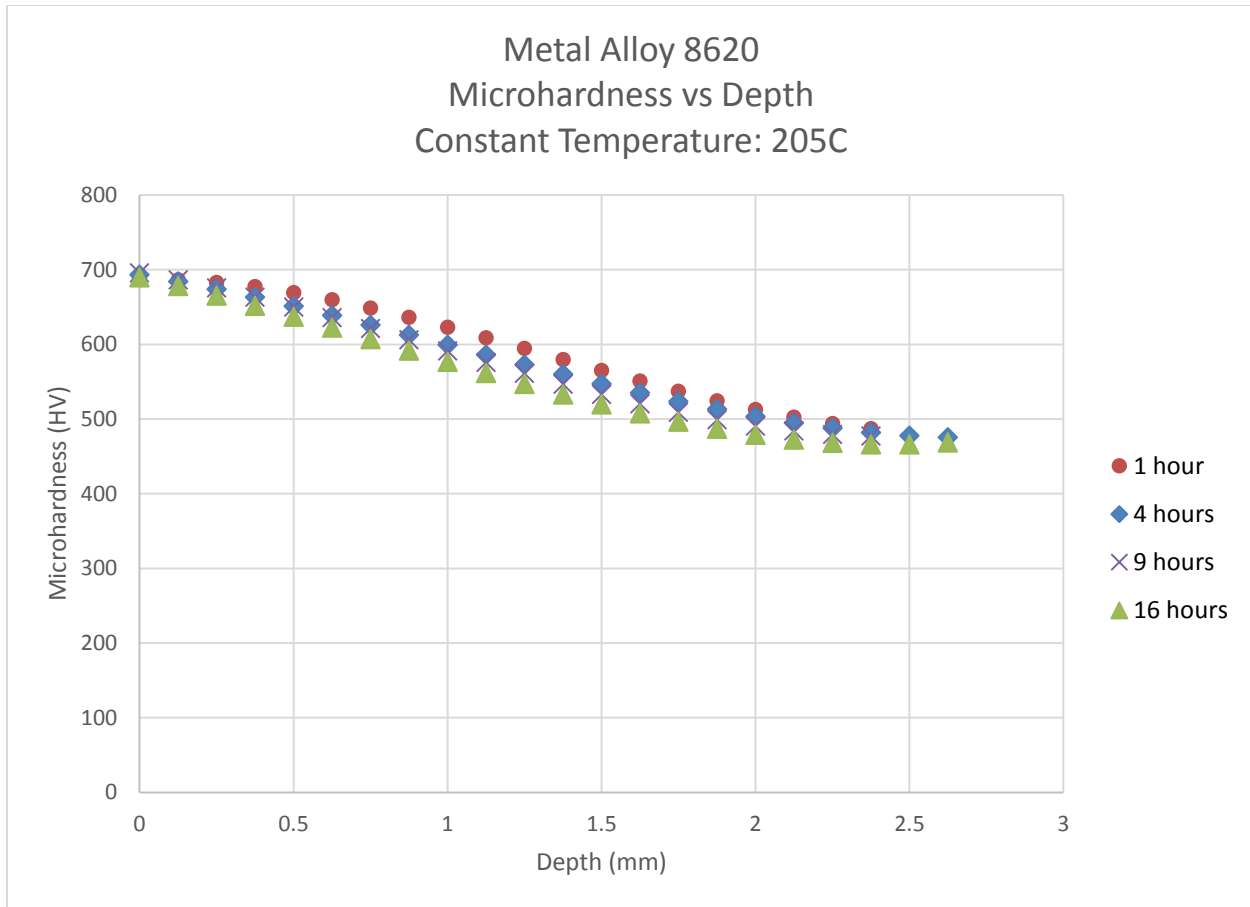


Figure 16: Microhardness (HV) vs. depth (mm) for AISI 8620, constant temperature and multiple times.

In the case of a constant temperature and varying time, it can also be seen that as the depth of the sample increases, the hardness decreases. As the time increases from one hour of tempering to sixteen hours, there is a decrease in the hardness. However, it can be inferred from the trends in Figure 15 and Figure 16 that the hardness is affected more by the change in temperature than it is by the change in time selected for tempering. The assumption to have selected a wide range in temperature for performing the tempering process and a smaller range for the tempering time for this project was correct.

After the hardness was obtained for the sample alloys, the respective carbon concentrations and microhardness were plotted against the depth of the sample. An example is shown below in Figure 17. For a complete list of these graphs plotted, please refer to Appendix C.6: Microhardness and OES vs. Depth Data.

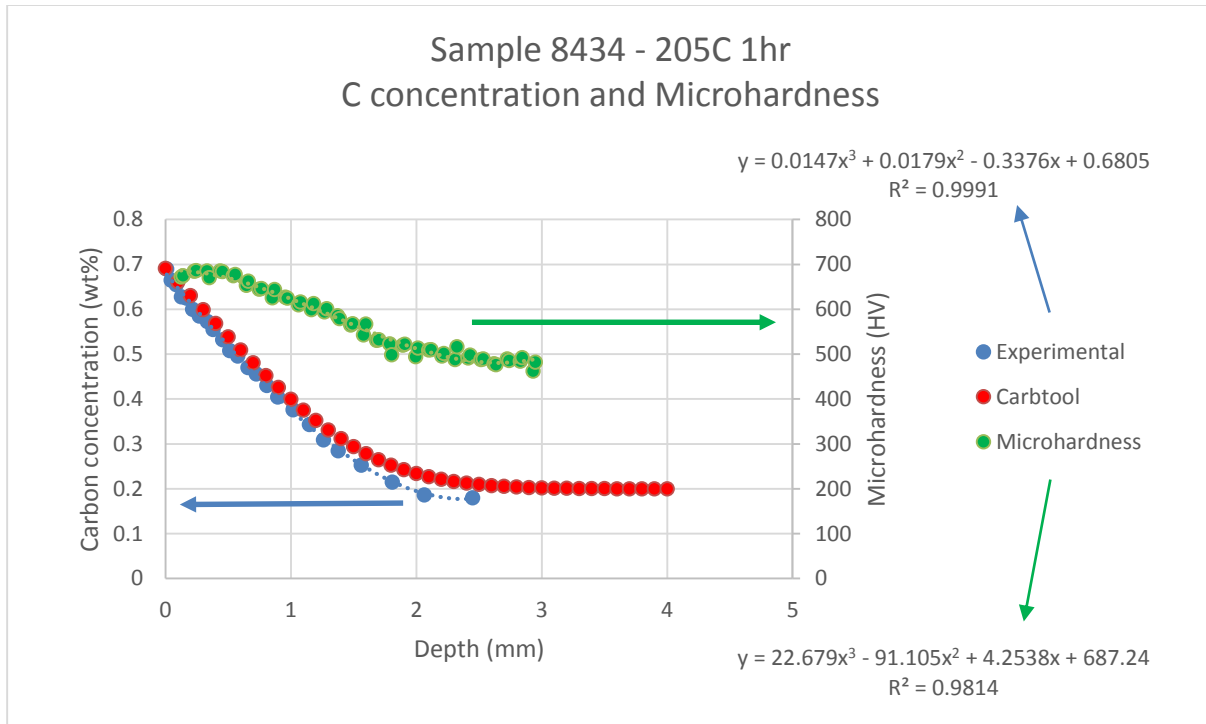


Figure 17: Carbon concentration (wt.%) and microhardness (HV) vs. depth (mm) for samples 8434 – 205°C 1hr.

This was done to display both microhardness and carbon concentration dependent on the depth, where an arbitrary depth could be selected to allow the microhardness to be plotted against the carbon concentration. The CarbTool© simulation trend is also displayed here.

After the carbon concentration and microhardness were plotted against depth, a trend line was fitted into each graph to obtain a polynomial equation. These equations were then used to plot the microhardness against carbon concentration, an example of which is shown in Figure 18 below. This was mostly done for alloys AISI 8620 and AISI 9310.

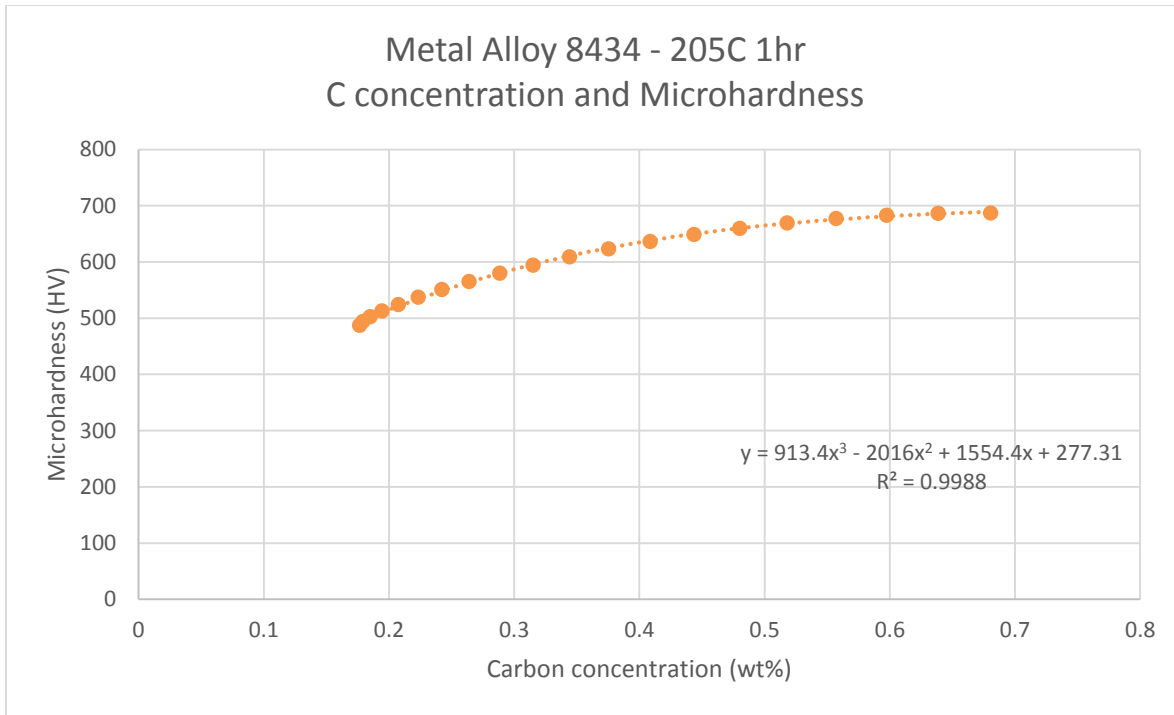


Figure 18: Microhardness (HV) vs. carbon concentration (wt.%) for sample 8434 – 205°C 1hr.

Figure 18 shows that as the carbon concentration of the alloy increases, the microhardness also increases before leveling out. The carbon concentration and the hardness are at their highest at the edge of the sample and both decrease as the depth increases. All other tables and graphs for the microhardness against carbon concentration are shown in Appendix C.7: Microhardness vs. Carbon Concentration Data.

The trends were once more analyzed for a constant time and multiple temperatures, and then again for a constant temperature and multiple times for alloys AISI 8620 and AISI 9310. These trends can be found in Appendix C.8: Microhardness vs. Carbon Concentration Trends. Below are examples of the trends for AISI 8620 at a constant time and multiple temperatures in Figure 19 and at a constant temperature and multiple times in Figure 20.

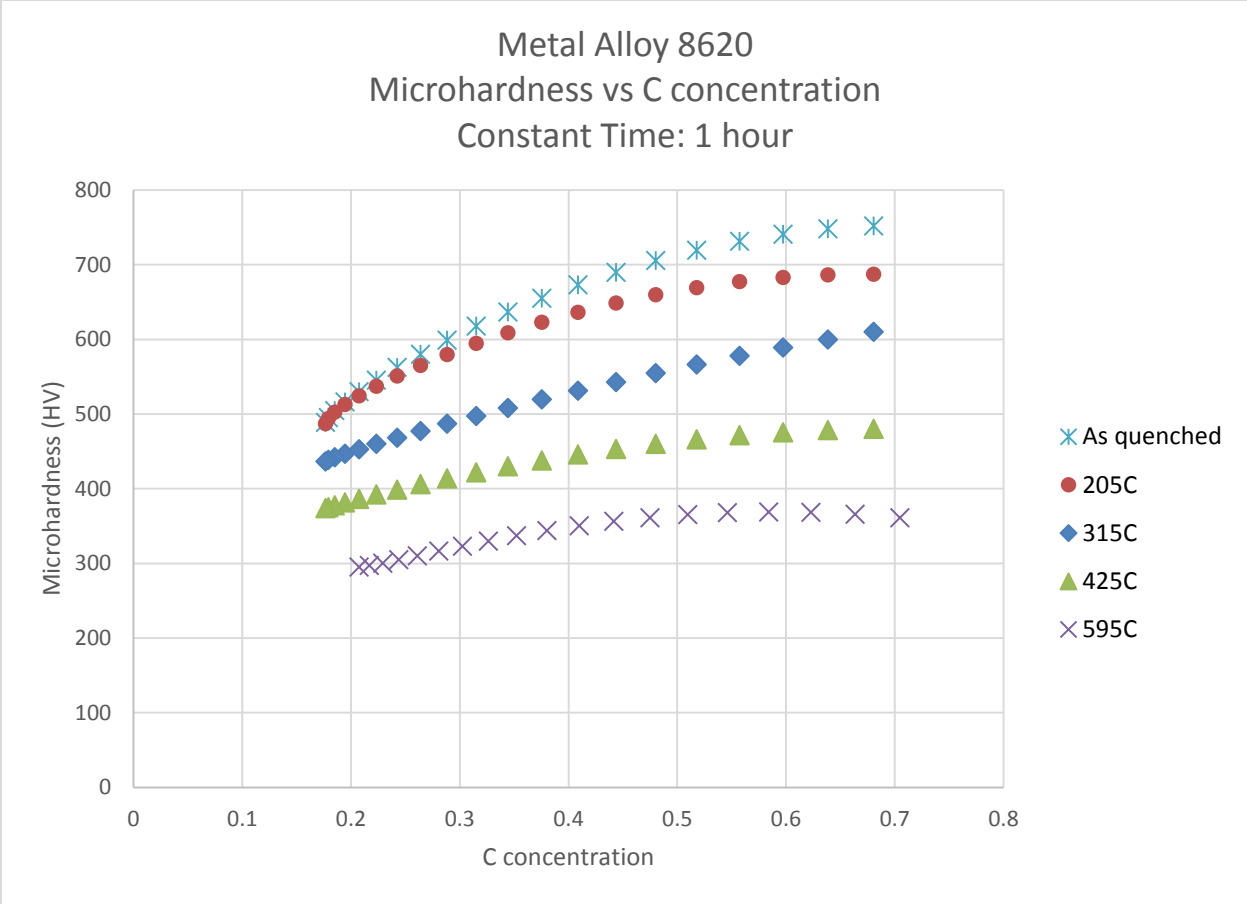


Figure 19: Microhardness (HV) vs. carbon concentration (wt.%) for AISI 8620, constant time and multiple temperatures.

The trends in Figure 19 show that as the temperature of the tempered sample increases, the hardness decreases. For all the different temperatures above, as the carbon concentration of the sample decreases, so does the hardness, which is in agreement with the literature.

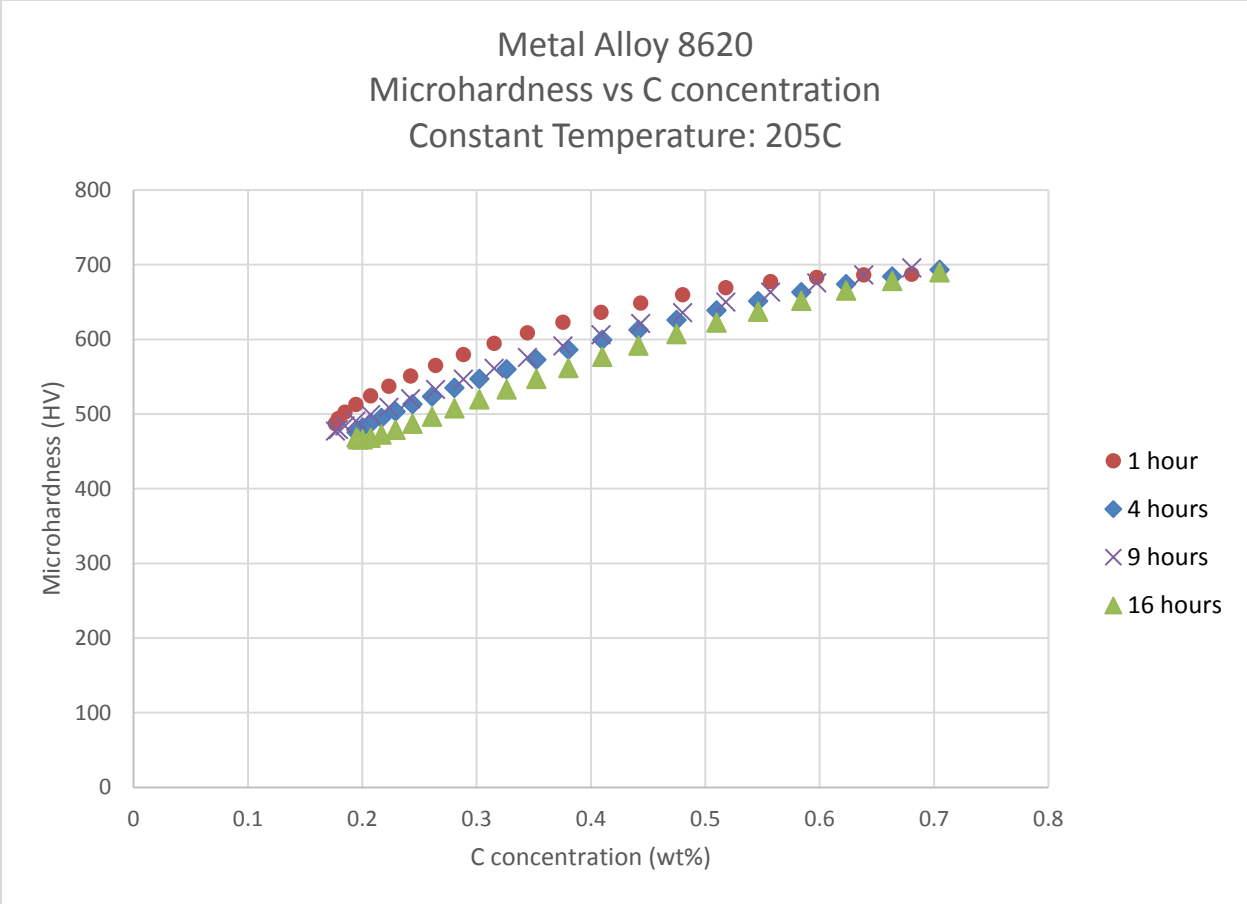


Figure 20: Microhardness (HV) vs. carbon concentration (wt.%) for AISI 8620, constant temperature and multiple times.

At a constant temperature and varying time, the graph in Figure 20 displays a marginal but sure trend that as time increases, hardness decreases. This, once again, is in agreement with the literature that the hardness of a sample is affected more by a change in temperature than by a change in time.

From the best fit polynomial line for the plot of microhardness against carbon concentration, a value of carbon concentration would then line up to a specific microhardness which would serve to complete the Hollomon-Jaffe parameter. For the sake of the Hollomon-Jaffe parameter, the carbon concentrations of 0.70, 0.50, and 0.30 were selected. These selected carbon concentration values would allow for the mathematical configuration of obtaining the C constant, which is specific to each alloy.

## 4.4 X-ray Diffraction

X-ray Diffraction was performed on the alloy AISI 9310 in order to accurately measure the amount of retained austenite in the alloy and to examine the phases in the sample. It was found that retained austenite was 16.17%. Figure 21 shows the results of the procedure with the values for each of the peaks shown on the graph.

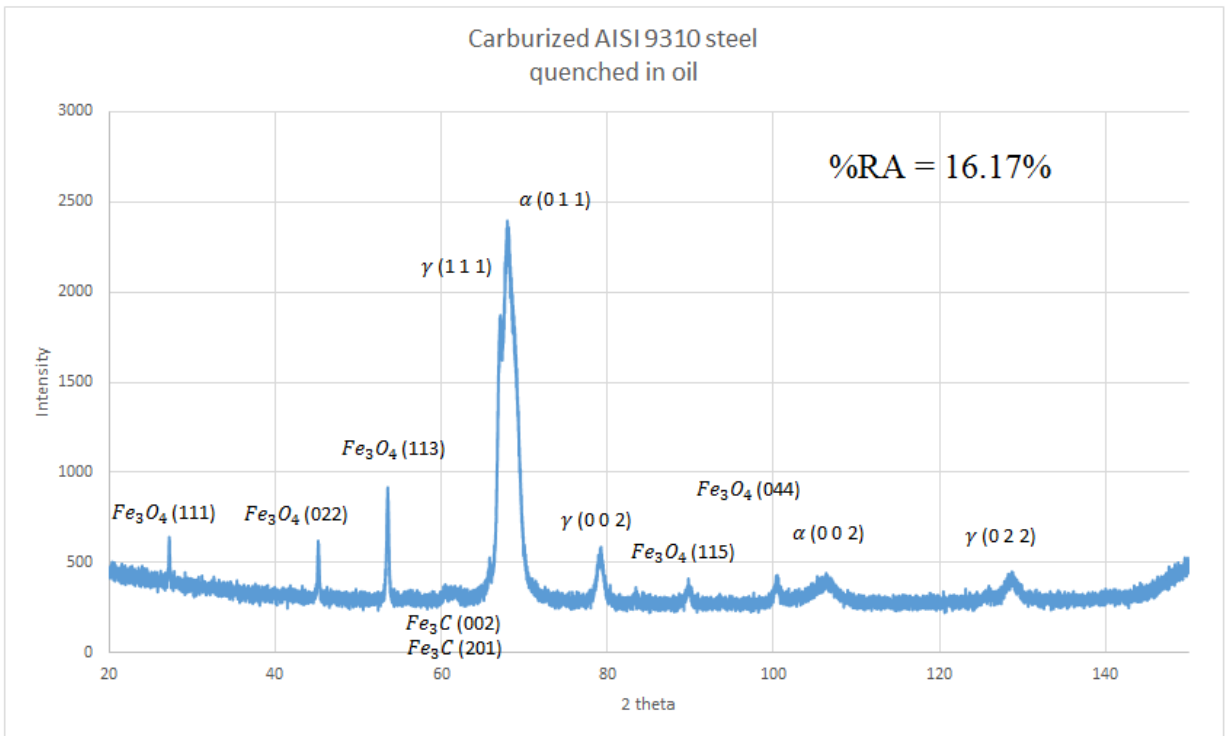


Figure 21: X-ray Diffraction for AISI 9310.

## 4.5 Photomicrograph

In order to take quality photomicrographs, the samples needed to be re-polished at 0.1 $\mu$ m. After re-polishing, a sonic cleaning was performed and the samples underwent an etching of a 2% nital solution, where the remainder of the solution was ethanol. All photomicrographs for this project were taken from samples of the alloy AISI 9310. This is because AISI 9310 is the only alloy in which retained austenite would be present. Alloy AISI 9310 is the only one with retained

austenite because the phase transition from austenite to martensite temperature is lower in AISI 9310 so it requires a lower temperature to transform to 100% martensite, leaving some retained austenite. Figure 22 shows a photomicrograph at a magnification of 5x on the edge of a sample.



Figure 22: Photomicrograph of AISI 9310 at 5x magnification.

It is harder to see it at the larger magnifications, but the darker spots are the tempered martensite crystals and the light colored areas are retained austenite crystals. Figure 23 is a photomicrograph at a higher magnification of 20x, again on the edge of the sample.

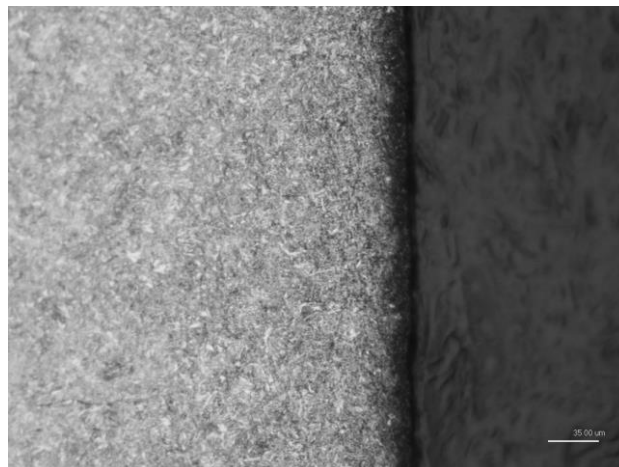


Figure 23: Photomicrograph of AISI 9310 at 20x magnification.

The differentiation between darker martensite crystals and light retained austenite crystals is easier to see at 20x than at 5x, but it still is not perfect. It is challenging to obtain photomicrographs at a magnification of 50x or higher because it is difficult to focus at the higher magnifications. Also, if the sample is not polished well enough, then at higher magnifications only part of the image will be in focus.

#### 4.6 Hollomon-Jaffe Parameter and Constant C for CarbTool©

The Hollomon-Jaffe parameter was obtained from equation 10 below.

$$HJP = T[\log(t) + C] \quad (10)$$

Three carbon concentrations were selected, 0.70, 0.50, and 0.30 wt.%C to plot the hardness against the natural log of time in hours. As shown below in Figure 24, this resulted in negative linear correlations.

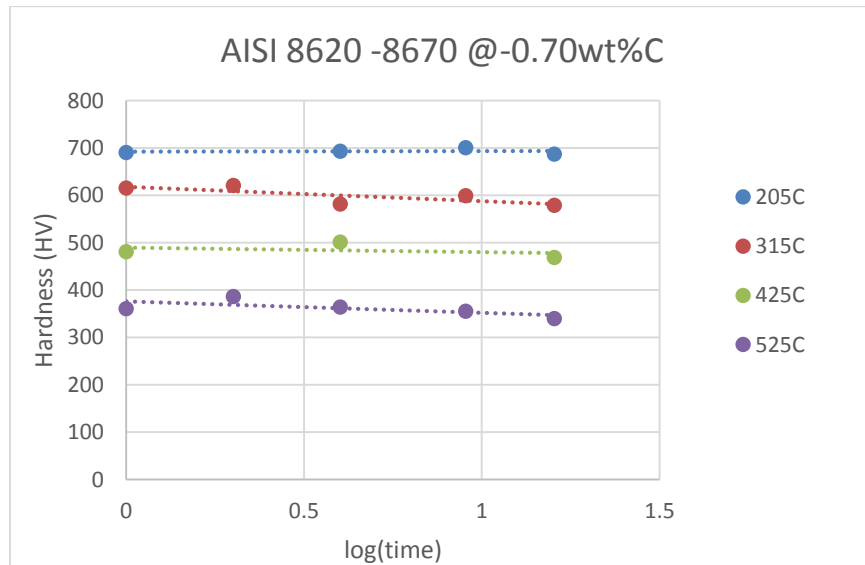


Figure 24: Hardness (HV) vs. log time for AISI 8670.

For the visualization of more Hollomon-Jaffe graphs at different carbon concentrations, please see Appendix C.9: Hollomon-Jaffe Data. In Figure 24, the microhardness for varying temperatures were plotted, however, the microhardness was not completed for 2 and 9 hours at 425°C for the sake of time.

In order to improve the existing CarbTool© for the process of tempering, the Hollomon-Jaffe constant (C) needed to be calculated. The constant C was determined for the three selected carbon concentrations i.e. 0.70, 0.50, and 0.30 wt.% for alloy AISI 8620. This was done by iterations of three combinations of time and temperature which have approximately the same hardness. The calculation of C was done using the programming software, Mathcad. The Mathcad calculations are shown in Appendix C.10: Mathcad Calculations. After obtaining the constant C at different concentrations, the graph was plotted for constant C vs. carbon concentration (wt.%) and it was determined that the relationship between them was linear, which can be seen in Figure 25.

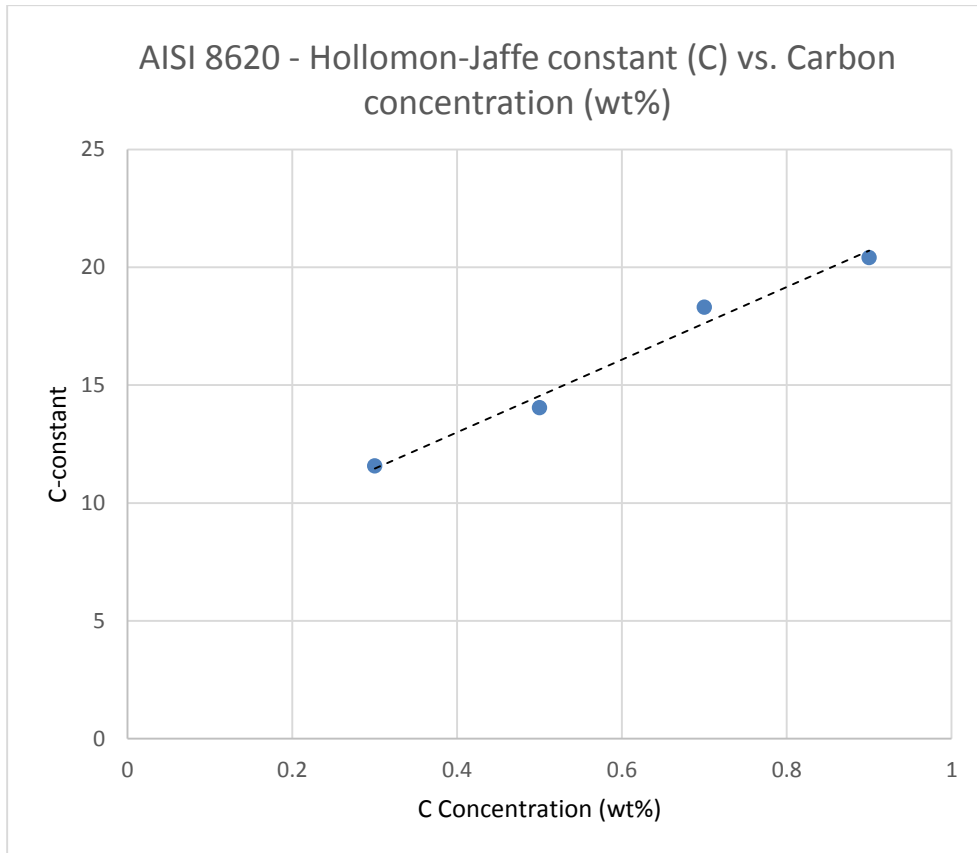


Figure 25: Hollomon-Jaffe constant (C) vs. carbon concentration (wt.%) for AISI 8620.

## 5.0 Conclusion

The goals of this project were to analyze hardness data using Hollomon-Jaffe parameter, to develop models for the prediction of microhardness profiles as a function of tempering time and temperature, and ultimately to optimize the tempering process by enhancing the simulation software CarbTool© in order to include the microhardness profile for the tempering process. Additionally, the microstructures of the alloys were to be analyzed in terms of phase transformation kinetics. As this project is an ongoing project in collaboration with CHTE, summarized here are conclusions and future plans for this project as well as recommendations for future work.

The analysis of the data using the Hollomon-Jaffe parameter was successful where the constant C values were obtained from the Hollomon-Jaffe equation using the different temperature and time combinations. Continued work should be done to develop better, more accurate models for the prediction of microhardness profiles as a function of tempering time and temperature. Further work should be done to improve the current model of predicting the microhardness profile for the tempering process. The resulting model from this project can be used for the following:

- Predicting the microhardness profile for tempered alloys AISI 8620, AISI 9310, AISI 1018, and AISI 5120.
- Comparison and analysis of the microhardness profile for any time-temperature combination.
- Reduction in the amount of experimental work for industry thus decreasing time to market and cost of any product.
- Overall optimization of the tempering process.

The microstructure of the steel was analyzed using photomicrographs and X-ray Diffraction. Future work for this project could be to create a model for the profile of the amount of retained austenite and incorporate said profile into CarbTool©.

## 6.0 References

- American Society for Testing and Materials International (2014). ASTM E975 - 13: Standard Practice for X-Ray Determination of Retained Austenite in Steel with Near Random Crystallographic Orientation.
- Black, M., Cook, R., Loveless, D., Rudnev, V., & Weiss, K. (1999). Induction tempering of steel. *Advanced Materials & Processes*, 156(2). doi: A55578903
- Brief Introduction to Scanning Electron Microscopy (SEM). ucr.edu.
- Center for Heat Treating Excellence. 2013, from <http://www.wpi.edu/Academics/Research/CHTE/>
- International ASM Handbook Committee (1986). Materials Characterization *ASM Handbook* (Vol. 10, pp. 380-393): ASM International.
- Davis, J. R. (1996). *Carbon and Alloy Steels*. Materials Park, OH: ASM International.
- Davis, J. R. (2002). *Surface hardening of steels: Understanding the Basics*. Materials Park, OH: ASM International.
- Oliveira, W. P. de, Savi, M. A., & Pacheco, P. M. C. L. (2013). Finite Element Method Applied to the Quenching of Steel Cylinders Using a Multi-Phase Constitutive Model. *Archive of Applied Mechanics*, 83(7), 1013-1037. doi: 10.1007/s00419-013-0733-x
- Eckelmeyer, K. H. (2012). Optical Emission Spectroscopy (OES) *Metals Handbook Desk Edition*: ASM International.
- Ericsson, T. (1991). Principles of Heat Treating of Steels: Cooling Media and Quench Intensity *ASM Handbook* (Vol. 4): ASM International.
- Etch Testing. Union Electric Steels: Forged and Cast Rolls.
- Friction, Lubrication, and Wear Technology. (1992) *ASM Handbook* (Vol. 18).
- Harichand, Chaturvedi, S., & Sharma, S. (2012). Optimization of Heat Treatment Process for 16MnCr5. *International Journal of Engineering Science and Technology*, 4(3), 998-1004.
- Hasan, H. S., Peet, M. J., Jalil, J. M., & Bhadeshia, H. K. D. H. (2010). Heat Transfer Coefficients During Quenching of Steels. *Heat and Mass Transfer*, 47(3), 315-321. doi: 10.1007/s00231-010-0721-4
- Heat Treating. (1991) *ASM Handbook* (Vol. 4).
- Heat Treating of Steel: Equipment for Tempering. (2002) *Metals Handbook Desk Edition* (pp. 970-982): ASM International.

Heat Treating of Steel: Mechanism of Quenching. (2002) *Metals Handbook Desk Edition* (pp. 970–982): ASM International.

Heat Treating of Steel: Tempering Procedures. (2002) *Metals Handbook Desk Edition* (pp. 970–982): ASM International.

Herring, D. H. (2005). A Discussion of Retained Austenite. *Industrial Heating's The Heat Treat Doctor*.

Hollomon, J. H., & Jaffe, L. D. (1945). Time-Temperature Relations in Tempering Steel. *Metals Technology* (162), 223-249.

Hollomon, J. H., & Jaffe, L. D. (1947). *Ferrous Metallurgical Design*: John Wiley and Sons Inc.

Home - Bodycote. (2013). from <http://www.bodycote.com/>

Hosford, W. F. (2005). *Physical Metallurgy*. Boca Raton, FL: Taylor & Francis.

Indacochea, J. E. Heat Treating of Steels and Metallic Materials: University of Illinois at Chicago: Civil and Materials Engineering Department.

Iron-iron carbide metastable phase diagram. (2013) (pp. Fe-C Phase/ Equilibrium Diagram). Scielo.

Kamp, A., Celotto, S., & Hanlon, D. N. (2012). Effects of Tempering on the Mechanical Properties of High Strength Dual-Phase Steels. *Materials Science and Engineering*, 538, 35-41. doi: <http://dx.doi.org/10.1016/j.msea.2012.01.008>

Krauss, G. (2005). *Steels: Processing, Structure, and Performance*. Materials Park, OH: ASM International.

Magner, S. H., De Angelis, R. J., Weins, W. N., & Makinson, J. D. (2002). A Historical Review of Retained Austenite and its Measurement by X-Ray Diffraction *Advances in X-ray Analysis* (Vol. 45).

Materials Science & Engineering: Student News - WPI. (2011). 2013, from <http://www.wpi.edu/academics/mte/news/asm-hts-2011.html#intelligent>

Metal Hardening / Metal Quenching / Metal Tempering. (2012). Retrieved 2013, from <http://www.metlabheattreat.com/metal-hardening-metal-quenching-metal-tempering.html>

Metallurgy; Findings from C. Gomes and Co-Researchers Advance Knowledge in Metallurgy. (2011). *Mining & Minerals Business*.

Morito, S., Tanaka, H., Konishi, R., Furuhashi, T., & Maki, T. (2003). The Morphology and Crystallography of Lath Martensite in Fe-C Alloys. *Acta Materialia*, 1789-1799.

- NANO 2000 Polisher: Instruction Manual. (2011): Pace Technologies.
- Neutral Hardening. (2013). 2013, from <http://www.bodycote.com/services/heat-treatment/harden-and-temper/neutral-hardening.aspx>
- Pappas, N. (2006). Calculating Retained Austenite in Steel Post Magnetic Processing Using X-Ray Diffraction (Vol. 4). B.S. Undergraduate Mathematics Exchange.
- Tempering. (2013). 2013, from <http://www.bodycote.com/en/services/heat-treatment/harden-and-temper/tempering.aspx>
- Totten, G. E. (2006). *Steel Heat Treatment: Metallurgy and Technologies* (2 ed.): CRC Press: Taylor & Francis Ltd.
- Vander Voort, G. F. (2004). Metallography and Microstructures *ASM Handbook* (Vol. 9): ASM International.
- Vermeulen, W. G., Van der Wolk, P. J., De Weijer, A. P., & Van der Zwaag, S. Prediction of Jominy Hardness Profiles of Steels Using Artificial Neural Networks. *Journal of Materials Engineering and Performance*, 5(1), 57-63. doi: 10.1007/BF02647270
- Virtanen, E., Van Tyne, C. J., Levy, B. S., & Brada, G. (2013). The Tempering Parameter for Evaluating Softening of Hot and Warm Forging Die Steels. *Journal of Materials Processing Technology*, 213(8), 1364-1369. doi: <http://dx.doi.org/10.1016/j.jmatprotec.2013.03.003>
- Wei, Y., Zhang, L., Liang, H., & Sisson, R. D. (2011). Gas and Vacuum Carburizing.

# Appendix

To access the appendix, please contact Professor Richard D. Sisson at Worcester Polytechnic Institute.